NJC

Accepted Manuscript

ROYAL SOCIETY OF CHEMISTRY

rsc.li/njc

View Article Online
DOI: 10.1039/C6NJ03893J

New Journal of Chemistry

ARTICLE

Thermo-Responsive Microgels Based in Encapsulated Carbon Quantum Dots

Received 00th January 20xx,
Accepted 00th January 20xx

DOI: 10.1039/x0xx00000x

www.rsc.org/

Bruno B. Campos,[a] Dragosav Mutavdžić,[b] Mira Stanković,[b] Ksenija Radotić,[b] Juan M. Lázaro-Martínez,[c] Joaquim C.G. Esteves da Silva,[a] Rafael Contreras-Cáceres,[d*] M. Soledad Pino-González,[d] Enrique Rodriguez-Castellón,[e] Manuel Algarra[e]*

In this work carbon quantum dots (CQDs) nanoparticles are synthesized from D-lactose using a hydrothermal method and then they are coated with polyethyleneglycol (CQDs@PEG).These particles exhibit a monodisperse spherical morphology with an average particle size of ~4 nm. Nuclear magnetic resonance (NMR) and Fourier transform infrared spectroscopy (FTIR) showed the presence of the hydroxyl groups from the ethylene glycol molecules grafted on the CQDs surface, which confirms that PEG was covalently attached to the nanoparticles surface. Fluorescence analysis demonstrates a shift in the emission at 495 nm after PEG coating. Modified carbon dots were introduced into thermo-responsive pNIPAM microgels. The resultant pNIPAM-CQDs@PEG hybrid system exhibits interesting fluorescent properties. Transmission electron microscopy (TEM), fluorescence microscopy, and energy-dispersed X-ray (EDX) spectroscopy confirm the incorporation of CQDs particles into the microgels. Finally, dynamic light scattering (DLS) analysis confirms that the further hybrid microgels based in pNIPAM are thermo-responsive, with a transition temperature similar to that for a system with an ionic component.

Introduction

Recently carbon quantum dots (CQDs) have become an attractive group of nanoparticles that have been used in several fields such as nanomedicine, bio-imaging, sensing, photo-catalyst, LED and energy conversion. Compared with other fluorescent species, such as semiconductor quantum dots (QDs) and organic dyes, the main advantages of CQDs are their high chemical stability, dispersibility in water, low photo-bleaching, and a strong biocompatibility with a low toxicity. [1-16]

To obtain CQDs from a variety of carbon sources, various synthetic approaches have been reported. They include microwave and hydrothermal oxidation, laser ablation, and arc discharge.[9,10,17-19] An important drawback of these procedures is a low quantum yield.[20,21] To overcome this problem, surface passivation is often used in order to enhance the fluorescence properties of CQDs.[22]

Several polyelectrolytes as poly(ethylenglycol) (PEG),[23-26] polyethyleneimine (PEI)[1] poly(ethylenimide)-co-poly(ethylene glycol)-co-poly(ethyl-enimide) (PPEI)[23] and 4,7,10-trioxa-1,13-tridecanediamine (TTDDA)[27] have been extensively used as effective coating agents for nanoparticles to enhance their properties. Moreover, the attachment of heteroatoms containing moieties into the surface of CQDs has been found to increase the fluorescence emission.[14,28] A chitosan/PEG mixture treatment has been also used as an attractive approach for preparation of passivated CQDs.[24] However, the mechanism of the fluorescence enhancement by coating agents still remains unknown.

In this work we present the synthesis of CQDs@PEG, obtained by an easy and efficient hydrothermal procedure. Our goal was a direct grafting of PEG molecules, through its OH groups, to the CQDs surface. It was expected to be achieved by formation of ester bonds between carboxylic groups of the CQDs surface and the -OH groups of PEG, which was demonstrated by solid NMR spectroscopy. Such modification allow us to obtain a component for nanocomposites/hybrid gel,[29,30] which was fabricated with N-Isopropylacryalmide (pNIPAM) polymer, resulting in a a photoluminescence thermo-responsive microgel (pNIPAM-CQDs@PEG), Fig. 1. As is well-known this microgel is a monodisperse colloidal particle which has a lower critical solution temperature (LCST) in water of 32 °C. This nanocomposite, pNIPAM-CQDs@PEG system, was synthesized by free radical polymerization of N-Isopropylacrylamide in presence of the CQDs@PEG nanoparticles. This stimuli-responsive microgel has been previously used for the encapsulation of several colloidal particles, as latex, SiO_2, Au, Fe_3O_4 or QDs for different purposes.[31-36] To our best

[a] Centro de Investigação em Química, Departamento de Química e Bioquímica, Faculdade de Ciências da Universidade do Porto, Porto, Portugal.
[b] Institute for Multidisciplinary Research, University of Belgrade, Kneza Višeslava1, 11000 Beograd, Serbia.
[c] Departamento de Química Orgánica & IQUIFIB-CONICET, Facultad de Farmacia y Bioquímica, Universidad de Buenos Aires, Junín 956 (1113) CABA, Argentina.
[d] Departamento de Química Orgánica, Facultad de Ciencias, Universidad de Málaga, Campus de Teatinos s/n, 29071 Málaga, Spain.
[e] Departamento de Química Inorgánica, Facultad de Ciencias, Universidad
[f] de Málaga, Campus de Teatinos s/n, 29071 Málaga, Spain.
† Footnotes relating to the title and/or authors should appear here.
Electronic Supplementary Information (ESI) available: Details of TG/DSC experiments and fluorescence spectra, TEM images of CQDs@pNIPAM particles and FE-SEM and EDX mapping analysis. See DOI: 10.1039/x0xx00000x

View Article Online
DOI: 10.1039/C6NJ03893J

knowledge, this is the first report concerning the fabrication of the hybrid photoluminescence pNIPAM-CQDs@PEG particles, which can be also used as stimuli response system toward temperature.

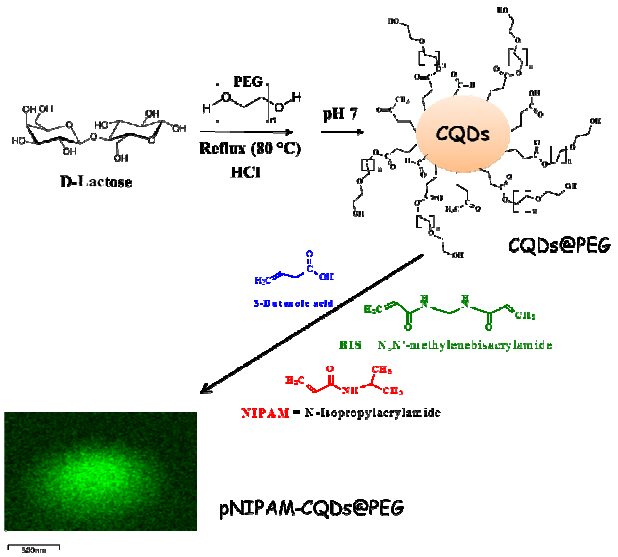

Figure 1. Schematic illustration of the synthesis route used to prepare luminescent pNIPAM-CQDs@PEG particles.

Results and discussion

Characterization of CQDs@PEG

CQDs@PEG nanoparticles were structurally characterized by *ss*-NMR experiments. Firstly, the ^{13}C CP-MAS spectrum of the CQDs@PEG solids presents well-resolved resonance signals corresponding to aliphatic or sp^3 region between 30-40 ppm and the sp^2 section around 210-170 ppm (Fig. 2A, B). In addition, the carbon signals of the PEG at 72.0 and 70.8 ppm in the pure state are not observed in the CQDs@PEG mixture, where its presence is missed in the baseline at 70 ppm as marked with an asterisk in the spectrum (Fig. 2C). The absence of PEG signal in the CQDs@PEG sample was due to the higher intensity of the resonance signals coming from the high degree of functionalization in the surface of PEG. In this sense, the ^{13}C signal of ordered structures produces an increase of the signal since in these regions the cross-polarization transfer from ^{1}H to ^{13}C is enhanced in comparison with disorder regions.[37]

In addition, the proton longitudinal relaxation times (T_1^H) of the PEG sample in the pure state and the CQDs@PEG were 3.63 s and 398 ms, respectively, which can explain the higher disorder of the polymeric segment in the CQDs@PEG mixture compared with pure PEG. Then, in order to do the correct assignment of the NMR signal, non-quaternary suppression (NQS) and cross-polarization polarization-inversion (CPPI) spectral edited experiments were performed. These results are included in Figure 2C-D, respectively. In the NQS spectrum, the carbons with non-hydrogen atoms directly bounded on the CQDs surface are observed at 208.7 and 182.1 ppm together with methyl carbons ($-CH_3$) at 30.3 ppm. In addition, the CPPI experiments allowed us to confirm that the signals at 32.6 and 40.2 ppm are assigned to methylene carbon ($-CH_2-$) and that the signal at 172.6 ppm is due to a formic acid ester carbon with a directly hydrogen atom linked, since it remains in the baseline ($H-CO_2R$). It is important to note from this analysis that the carbonyl carbon at 208.7 ppm is assigned to a ketone carbon and not to an aldehyde carbon.

Furthermore, the signal at 183.1 ppm corresponds coming to another ester carbon ($-CO_2R$), coming from the esterification reaction between the carboxylic acid with the hydroxyl groups from the PEG polymer. The same esterification process can be observed for the signal at 172.6 ppm, which allowed the incorporation of formic acid to the PEG polymer. The carboxylic acid groups have their origin from the oxidation of the aldehyde moieties during the synthesis of the CQDs. With the analysis of these NMR results we can confirm that the hydrothermal treatment of D-Lactose at 80 °C produced formic and levulinic acid products, from the acid decomposition of 5-hydromethylfurfural [38-40] that can be bounded through an esterification reaction with the hydroxyl groups in PEG molecules, according with both solid and liquid state NMR (see the inset in Fig. 2E).

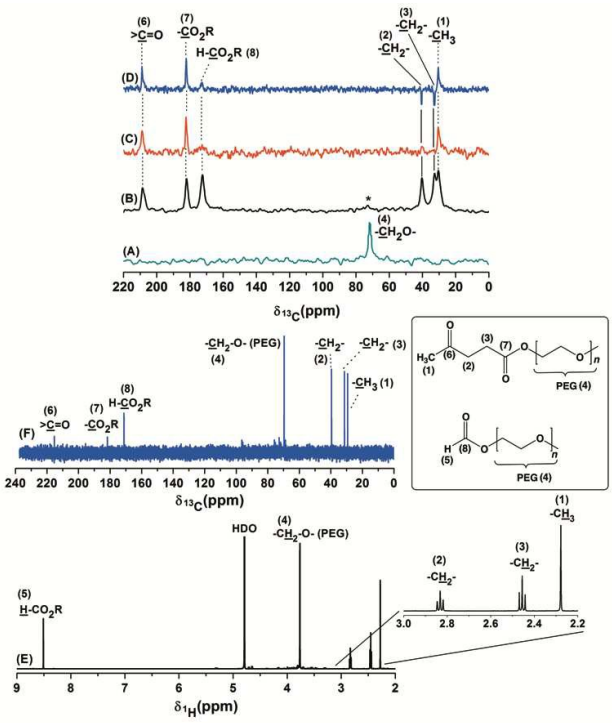

Figure 2. ^{13}C CP-MAS spectra: **A**) poly(ethyleneglycol)=PEG and **B**) CQDs@PEG particles. Edited CQDs@PEG spectra: **C**) non-quaternary suppression; **D**) cross-polarization/polarization inversion. CQDs@PEG spectra (D_2O): **E**) ^{1}H-NMR and F) ^{13}C-NMR.

In addition, the solution-state NMR resulted from the CQDs@PEG dispersed in D_2O showed a 49% of functionalization with the mineralization products (levulinic and formic acids), a 32% of PEG and a 19% corresponding to residual monosaccharide compounds in a mixture of two β-anomers (δ^1H: 4.71 and 4.65 ppm (*d*, ^3J = 7.9

View Article Online
DOI: 10.1039/C6NJ03893J

Hz)) and two β-anomers (δ^1H: 5.32 and 5.29 ppm (*d*, ^3J = 3.8 Hz)) having into account the area of the ^{1}H-NMR signals (Fig. 2E-F). The rest of the proton signals corresponding to the monosaccharide structures resonated around 3-4 ppm in the level of the ^{1}H NMR spectrum baseline. Moreover, the ^{13}C NMR spectrum in D_2O for the CQDs@PEG allowed visualizing the carbon resonance signals at 69.6 ppm corresponding to the PEG structure, which cannot be observed in the ^{13}C CP-MAS of the same material, since, as was previously mentioned, the cross-polarization step used in the ^{13}C spectrum acquisition in the solid-state increase the signal from the ordered regions.

Finally, Figure 3 includes solid-state 2D ^{1}H-^{13}C heteronuclear correlation (HETCOR) experiment performed for the CQDs@PEG nanoparticles. As can be observed the different ^{13}C nuclei correlated with the protons that were directly linked (*correlations* E-D) or nearby (A-C), and allowed us to study the connectivity of the different segments, inset in Fig. 3). In general, the hydrocarbon chains attached to the CQDs@PEG nanoparticles interact with protons at 2.50 and 1.70 ppm, however only the formic acid ester carbon (172.6 ppm) presents a strong interaction with its bounded proton at 8.70 ppm, which confirms its presence according with the solution-state NMR results where the proton of the formic acid segment (H-CO_2R) appears as a singlet at 8.52 ppm (Fig. 3E-F). Then, the signal coming from the other ester groups at 183.1 ppm only presents a correlation with the nearby hydrogen atoms of the methylene moieties at 2.09 ppm in the proton dimension (Fig. 3, *correlation* B).

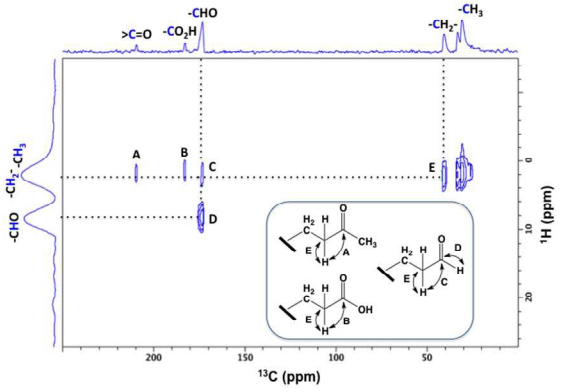

Figure 3. Solid-state 2D1H-^{13}C HETCOR spectrum for CQDs@PEG.

The absence of a correlation between carbons with protons at high frequency values (10-15 ppm) in the HETCOR spectrum, even at contact times of 200-500 μs, clearly demonstrates that the carbon at 183.1 ppm is assigned to an ester carbon and not to a carboxylic acid, since these kind of interactions are generally observed in the 2D HETCOR experiments in the solid-state.[41,42] With these evidences, the interaction concerning the PEG and the mineralization products coming from the oxidation of D-Lactose was demonstrated.

Consequently PEG provides surface functionality, which leads to an enhanced chemical and photoluminescence stability, which were confirmed by measurement of fluorescent intensities, showing a high luminescence and bright orange color after 2 months.

The size and morphology of the synthesized CQDs@PEG were analyzed by TEM (Fig. 4). As can be observed CQDs@PEG showed a good monodispersity resulting spherical nanoparticles, with a measured average size of 4.13±0.77 nm.

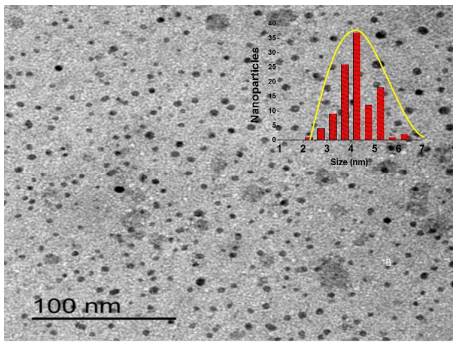

Figure 4. TEM image of CQDs@PEG nanoparticles with an average diameter of 4.13 ± 0.77 nm.

FTIR spectra for PEG, CQDs and CQDs@PEG nanoparticles were obtained and compared (Fig. 5A-C). PEG shows the characteristics stretching modes assigned to the peaks comprised between 1050-1150 cm^{-1} (C-O-C), 1000-1260 cm^{-1} (C-O) and 3200-3600 cm^{-1} (O-H), Fig. 5A. CQDs exhibited the characteristic vibrational mode of C=O (1600 cm^{-1}) on the surface. The band centered at 1108 cm^{-1} is ascribed to the C-H deformation sand stretching vibrations of C-O (ether) and C-C, pertaining to carbohydrates. A very broad strong band at 3398 cm^{-1} and the peak centered at 1108 cm^{-1} represent the stretching vibrations and in-plane bending vibration of OH (Fig. 5B). The spectrum of CQDs@PEG shows a prominent band at 3436 cm^{-1} that represents the stretching vibration of O-H groups. Bands at 2937 cm^{-1} (sym) and 2801 cm^{-1} (asym) indicate the presence of aliphatic -CH_2- groups, which are confirmed by the C-H bending mode at 1338 cm^{-1}. A weak band at 2151 cm^{-1} is assigned to the combination frequency of (C-H+C-C). The band at 1715 cm^{-1} can be assigned to a -C=C- stretching mode, which was also confirmed by a band at 1408 cm^{-1}.

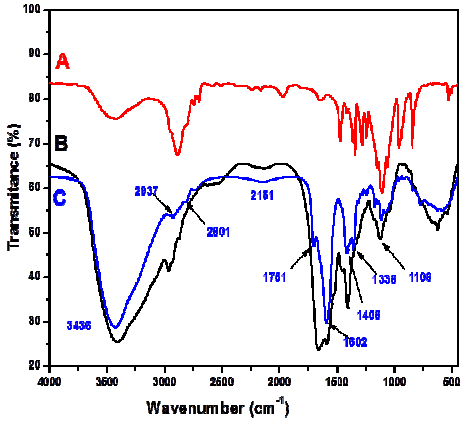

Figure 5. FTIR spectra of **A**) PEG, **B**) CQDs and **C**) CQDs@PEG.

View Article Online
DOI: 10.1039/C6NJ03893J

Two bands at 1414 and 1346 cm^{-1} represent the bending modes of the -CH_2- groups. A weak band at 1346 cm^{-1} is linked the combination frequency of (CH+OH) groups. An important finding is that the FTIR spectrum for CQDs@PEG shows a characteristic absorption band for a -C-O-C- stretching vibration at 1115 cm^{-1}. This supports the expected cross-linking between CQDs and PEG. A characteristic band at 1605 cm^{-1} is ascribed to the carbonyl groups (stretching mode of C=O from the surface of CQDs) stemming from the lactose content. The bands at 1585 cm^{-1} and 1664 cm^{-1} for CQDs of similar intensities, are assigned to the keto C=O and/or aldehyde C=O, respectively, which are present on the surface of CQDs. On the spectrum of CQDs@PEG, both bands shift to the longer wavelengths and are visible at 1593 cm^{-1} and 1704 cm^{-1} respectively. This may be due to the change of the C=O environments, from more to less branched, which causes shift to the low energy region in IR. The bands due to the stretching of C-O/C-O-C appear between 1214 and 1013 cm^{-1}. The shift to lower frequencies compared to the normal modes is explained by the interactions of PEG with the surface of CQDs. Another important band located at 1108 cm^{-1} in the spectra of both PEG and CQDs@PEG, is assigned to -OH in primary alcohol.

We also confirm the presence of the PEG group onto the CQDs particles by XPS investigations. The C 1*s* core energy level spectrum of CQDs@PEG (Fig. 6A) is decomposed into four different contributions, corresponding to C-C at a binding energy of 284.8 eV, C-OH and C-O-C at 286.1 eV, carboxylate at 288.4 eV and surface carbonate at 290.4 eV. Meanwhile the O 1*s* core energy level can be decomposed into two contributions (Fig. 6B) at 530.8 (C=O) and 532.8 (C-O) eV. The C 1*s* core level spectrum of CQDs is also composed of four contributions at 284.8, 287.3, 289.0 and 291.0 eV assigned to C-C, C=O, carboxylate and carbonate, respectively. However, the shape of the spectrum is different to that of CQDs@PEG (Figure 6C), showing the contribution at high binding energy with a very low relative intensity.

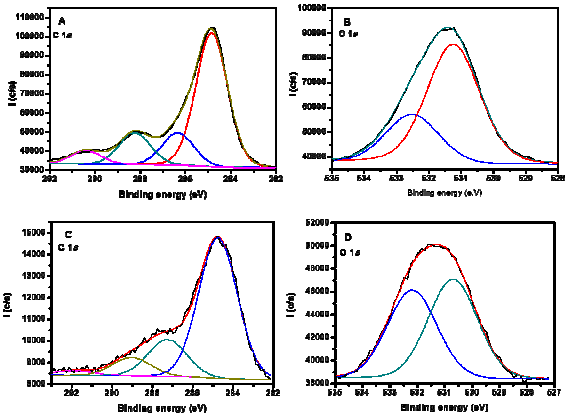

Figure 6. A) C 1*s* and B) O 1*s* core level spectra of CQDs@PEG system; C) C 1*s* and D) O 1*s* core level spectra of CQDs particles.

The O 1*s* core level spectrum of CQDs (Fig. 6D) also shows differences, where two contributions at 530.7 and 532.2 eV are also observed, but the contribution at low binding energy derived from the presence of C=O, carboxylate and carbonate groups (530.7 eV) presents a lower relative intensity than that observed in the case of sample CQDs@PEG. This is due to the practically absence of the contribution due to the presence of carbonates.

The XPS data indicate that the different functional groups shown in Fig. 1 for CQDs@PEG nanoparticles are presented at the surface and with a relevant contribution due to carboxylate and carbonate groups that are poorly observed in the C 1*s* spectrum of sample CQDs. The O 1*s* spectrum also supports the same observation, where the relative intensity of the contribution at low binding energy (530.7 eV) decreased in the case of sample CQDs. The C/O atomic ratios are 3.86 and 4.72 for CQDs@PEG and CQDs, respectively. The higher observed C/O ratio for CQDs@PEG is due to the incorporation of ethylene glycol moieties to the external surface of the CQDs nanoparticles.

The excitation-emission landscapes for CQDs and CQDs@PEG systems are shown in Figure 7A-B. Examples of the overlapped emission spectra, for CQDs and CQDs@PEG, after 365 nm excitation, are showed in Figure 7C. The obtained spectra are complex and the one for CQDs@PEG is considerably broader than that for the carbon dots alone. The emission maximum is produced at 455 nm for CQDs and at 495 nm for CQDs@PEG. The results of Factor analysis of the emission profiles for pure CQDs and CQDs@PEG are shown in Figure 7D. To probe the functionalization of CQDs by PEG, their quantum yields (QYs) were measured, obtaining an enhancement of it (from 8.1 to 11.1%). This result indicates that he surface passivation stabilizes the surface energy traps and makes them emissive. The emission spectrum of pure CQDs contains two components with the maxima 430 and 480 nm, corresponding to the two emitting structures in the CQDs. After the introduction of PEG, other components are formed and they emit at 455 nm and 510 nm. The number of components are unchanged, but a broadening of the spectrum for CQD@PEG and are shift of the component emission maxima, in comparison with the pure CQDs, can be observed. The red shift may be additionally caused by aggregation of the CQDs@PEG resulting in large aggregates.[43]

The fluorescent lifetimes for raw CQDs and CQDs@PEG were calculated. The fluorescent decay curve was fitted to a three exponential decay model with a satisfactory goodness of the fit (χ^2 = 1.177). The fluorescence lifetimes of our materials are listed in Table 1. Although in steady state fluorescence there is no change in the number of emission components in the spectra of CQDs@PEG particles in comparison with that of pure CQDs, the three lifetimes in the fluorescence decay of the complex vs two lifetimes for pure CQDs must be a result of the PEG binding to CQDs.

The short life times are similar to those of QDs and they reveal the radiative recombination nature of excitations.[44] The average fluorescence lifetime of the CQDs@PEG (5.93 ns, similar that for CQDs 5.12 ns) in the nanosecond range suggests that the synthesized CQDs@PEG is very suitable for sensing applications. The fluorescence lifetime decay analysis is presented in Supplementary Information (Fig. S2).

View Article Online
DOI: 10.1039/C6NJ03893J

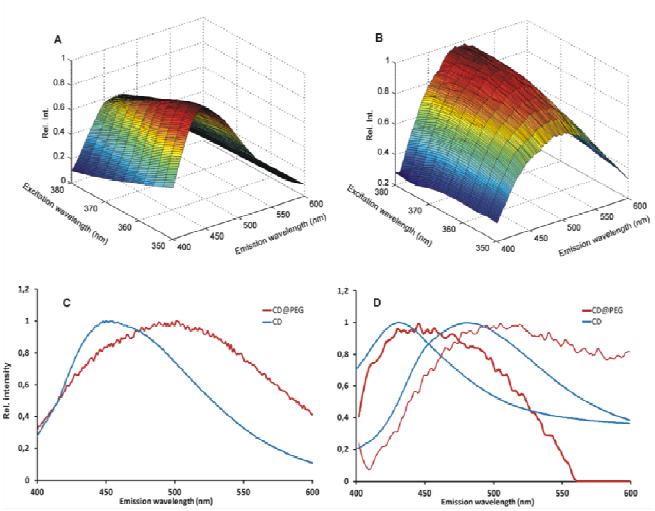

Figure 7. Excitation-emission landscape for raw spectra: **A**) CQDs and **B**) CQDs@PEG. **C**) Emission spectra of CQDs and CQDs@PEG for excitation at 365 nm. **D**) Estimated emission profiles for CQDs and CQDs@PEG obtained by MCR-ALS.

Table 1. Fluorescence lifetimes (ns) of CQDs and CQDs@PEG

	CQDs	CQDs@PEG
A	$1.50\times10^{2} \pm 0.18$	59.292 ± 0.92
B_1	$1.05\times10^{3} \pm 0.30$	$1.47\times10^{4} \pm 0.59$
B_2	$3.02\times10^{2} \pm 0.22$	$1.06\times10^{4} \pm 0.17$
B_3	-	$2\times10^{3} \pm 0.06$
τ_1	2.41 ± 0.03 (41.3%)	1.97 ± 0.01 (28 %)
τ_2	7.84 ± 0.05 (58.7%)	4.71 ± 0.02 (47%)
τ_3	-	10.56 ± 0.06 (25 %)
χ^2	1.155	1.177

Encapsulation of CQDs@PEG into pNIPAM

A further step of our research was the fabrication of a photoluminiscent microgel by the encapsulation of CQDs@PEG nanoparticles within pNIPAM microgels. As was mentioned in the experimental section, CQDs@PEG nanoparticles were initially treated with 3-butenoic acid. 3-BA is a bifunctional molecule that contains a carboxylic group, which bound on the particle surface, and it also contains a terminal double bond, which supplies surface vinyl functionality. For the pNIPAM encapsulation, the presence of this terminal double bond is critical because through this vinyl group the N-Isopropylacrylamide molecules are able to polymerize by free radical polymerization, thus finally resulting in a hybrid colloidal structure.[34,36] Well-organized pNIPAM-CQDs@PEG microgels are shown in Figure 8A. They exhibit a narrow size distribution with a mean value of ~350 nm. It is important to mention that at this magnification level the CQD@PEGs nanoparticles inside the microgel cannot be observed. Figure S3A includes representative high magnification TEM image of the individual pNIPAM-CQDs@PEG microgel nanoparticles. As is shown the pNIPAM microgel contains well-dispersed CQDs particles inside the polymer network. TEM image also show CQDs deposited on the microgel surface, as well as CQDs remaining outside the microgel, probably due to the need of an extra centrifugation step. In order to confirm the importance of the 3-BA treatment, the pNIPAM polymerization was performed in presence of CQDs@PEG particles without 3-BA treatment. This process resulted in CQDs@PEG aggregates encapsulated by an inhomogeneous structure with no-defined microgel morphology, as can be seen in TEM images (Figure S3B).[34]

The photoluminescence nature of the PNIPAM-CQDs@PEG system was confirmed by optical fluorescence microscopy images. Figure 8B shows fluorescence images of the pNIPAM microgels. As can be observed microgels possess fluorescence intensity that demonstrates the fabrication of pNIPAM microgels with luminescence capabilities by incorporation of CQDs. Figure S4 shows EDX mapping images for C and N of a pNIPAM-CQDs@PEG system. The atomic concentrations were as follows: 45.36 % C, 4.47 % N and 1.87 % O. For comparison the EDX spectroscopy analysis for CQDs@PEG resulted in 21.75 % in C, and 1.53 % O. The difference in the C and N can be attributed to the presence of the pNIPAM microgel.

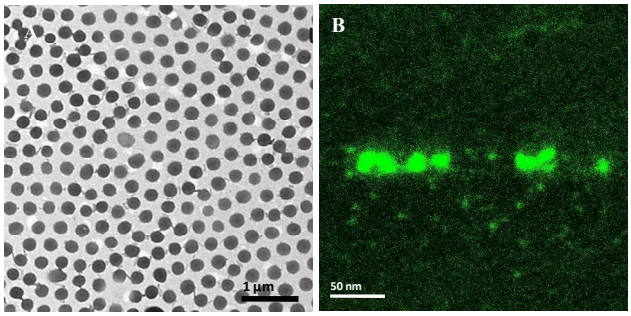

Figure 8. A) TEM image of the hybrid PNIPAM-CQDs@PEG nanoparticles **B**) Confocal fluorescence microscopy image of the PNIPAM-CQDs@PEG nanoparticles.

The QY of pNIPAM-CQDs@PEG decreased to 8.6 % compared with the raw CQDs@PEG (11.1 %). This can be explained by the reabsorption of the emitted light in the microgels containing CQDs@PEG.

The thermo-responsive properties of the pNIPAM-CQDs@PEG microgels were analyzed by DLS measurements. Figure 9A displays the variation of the hydrodynamic diameter of the pNIPAM-CQDs@PEG system when the temperature varied from 25 to 45 °C. It is seen that the particles shrink continuously with the increasing temperature as a consequence of the temperature-dependent.[40] A well-defined volume transition is observed between these temperatures. pNIPAM-CQDs@PEG leads to stable hybrid microgel with size between ~200 nm, in the collapsed state and ~750 nm in the swollen state. As was previously mentioned, pNIPAM has a LCST in water of 32 °C.[41] Interestingly, for these pNIPAM-CQDs@PEG microgels; the LCST is shifted toward higher temperatures. This LCST can be calculated as the minimum of the first derivative of the size versus the temperature. Figure 9B represents the δ(DH)/δ(temperature) as a function of temperature. As observed,

View Article Online
DOI: 10.1039/C6NJ03893J

the LCST shifts to 35 °C. This shift in the temperature could be explained by the presence of the -OH groups of PEG inside the microgel network. More of PEG groups lead to a higher charge density, which increases the electrostatic component between oxygen atoms that tends to swell the microgel. This repulsive electrostatic component competes directly against the temperature and causes that to shrink microgel the higher temperatures are needed.[46] Hence, a higher temperature is necessary to reach the same shrinking ratio.

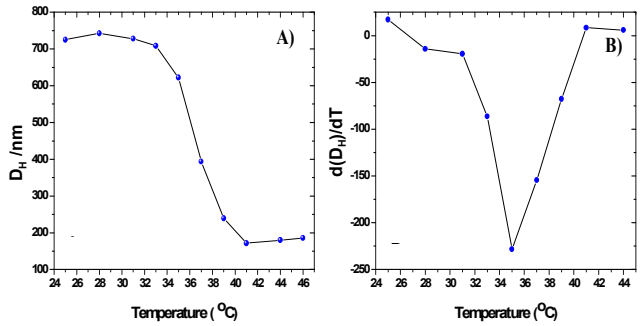

Figure 9. A) Variation of the hydrodynamic diameter of pNIPAM-CQDs@PEG with temperature. **B**) Representation of δ(DH)/δ(Temperature) of pNIPAM-CQDs@PEG nanoparticles in function of temperature.

Experimental

Materials

Poly(ethylene glycol) (PEG, MW = 3350), acetone (≥98.5 %), 3-butenoic acid (3-BA, 97%), 2,2'-azobis-(2-methylpropionamidene) dihydrochloride (V50,97%), D-Lactose (≥98%), N,N'-methylenebisacrylamide (BIS, ≥99.5%), N-Isopropylacrylamide (NIPAM, 97%), hexadecyltrimethylammonium bromide (CTAB, ≥99%) and Hydrochloric acid (37%) were purchased from Sigma-Aldrich Química S.A. (Spain) and used without further purification. In all experiments deionized H_2O was used (Milli-Q).

Synthesis of Carbon quantum dots coated by PEG

PEG (50 mg) was first dissolved in acetone (3 mL) at a room temperature under constant magnetic stirring for 5 min. To synthesize CQDs we followed a protocol previously described in the literature with some modifications in the final process.[9] Briefly, 100 mL of D-Lactose (1M) were treated with 50 mL of HCl (37 %) under reflux at 80 °C and stirred for 1 h. After that, the solution was neutralized with NaOH (1M), filtered and finally dialyzed (cellophane membrane using a MW CO 12.000-14.000 Da dialysis tube from Medicell International) with H_2O for 24 h to obtain CQDs. For the preparation of CQDs@PEG, 1 mL of the acetone solution of PEG was added to 1 mL of the CQDs dispersion, and stirred for 3 h. After that, it was centrifuged and the solvent evaporated in vacuum at 50 ºC for 12 h. The sample obtained is referred to as CQDs@PEG throw the manuscript.

Synthesis of pNIPAM-CQDs@PEG particles

The encapsulation of CQDs within pNIPAM microgel was performed following the procedure reported previously.[34] Briefly, CQDs@PEG nanoparticles (150 mg) were dispersed by sonication in a vial containing 10 mL of water. Then the vial was immersed in a water bath at 70 °C. After that, 80 µL of 3-BA were added under magnetic stirring to introduce terminal double bonds on CQDs surface. [34,36] This solution was stirred for 1 hour, and they were centrifuged for 30 min at 8000 rpm in order to remove the 3-BA excess. To reduce aggregation effects, 200 µL of 0.2 M CTAB were added to the colloidal solution before the centrifugation process. After that, the supernatant was discarded and the precipitate was re-dispersed with 10 mL of water and sonicated for 15 min. For the pNIPAM polymerization, the obtained solution of the modified CQDs was put into a three-neck round-bottom flask and heated up to 70 °C under magnetic stirring (350 rpm) and N_2 atmosphere. Subsequently, 0.226 g of NIPAM (monomer reagent which polymerize to form microgels) and 0.031 g of BIS (a cross-linker agent for the NIPAM monomer) were added to the modified CQDs colloidal dispersion. The mixture was stirred for 15 min, and the polymerization was initiated by adding 100 µL of 0.1 M V_{50} (the radical initiator). Then the N_2 flow stopped, and the polymerization was maintained for 2 h. Finally, the resulting white mixture was cooled down and diluted in water (25 mL). To remove small oligomers, unreacted monomers as well as the CQDs-free microgels produced during the polymerization process it was centrifuged (30 min at 4000 rpm) and the final precipitate was re-dispersed in water. This purification process was repeated 5 times. To better understand the preparation of all particles; Figure 1 illustrates the different pathways followed to obtain CQDs@PEG nanoparticles as well as the encapsulated pNIPAM-CQDs@PEG microgels.

Characterization Methods

Morphological analysis was carried out by TEM (EOL JEM1400) operating at acceleration voltage of 80 kV. For particles TEM analysis the samples were prepared by pipetting a small drop of colloids onto a TEM grid. The FTIR spectra were recorded on a Spectrum 1000 Perkin-Elmer Fluorescence spectra of CQDs@PEG were collected using a Fluorolog-3 spectrofluorimeter (JobinYvon Horiba, Paris, France) equipped with a 450W Xe lamp and a photomultiplier tube. QYs were obtained using Rhodamine 6G ($\Phi = 0.93$ in methanol, n=1.329 and λ_{ex} = 535 nm) as reference; CQDs and CQDs@PEG were dissolved in deionized water (n =1.33) and by 1, leads to obtain the QY of both nanoparticles

$$QY_{CDs} = QY_{st}\left[\frac{(dI/dA)_{CDs}}{(dI/dA)_{st}}\right]\left(\frac{n^2_{CDs}}{n^2_{st}}\right) \quad (1)$$

where I is the area under the fluorescence curves and A is the corresponding absorbance.[47,48]

XPS studies were performed on a Physical Electronic PHI 5700 spectrometer using non-monochromatic anode (Mg-K_α radiation with 300 W, 15 kV and 1253.6 eV) for analyzing the core-level signals of the elements of interest with a hemispherical multichannel detector. The spectra of powdered samples were recorded with a constant pass energy value at 29.35 eV, using a 720 µm diameter circular analysis area. The X-ray photoelectron spectra obtained were analyzed using PHI ACESS ESCA-V6.0F software and processed using MultiPak 8.2B package. The binding energy values

View Article Online
DOI: 10.1039/C6NJ03893J

were referenced to adventitious carbon C1s signal (284.8 eV). Shirley-type background and Gauss-Lorentz curves were used to determine the binding energies. DLS of PNIPAM-CQDs@PEG microgles was determined using a Zetasizer Nano ZS (Malvern Instruments, U.K.) equipped with a 4 mW HeNe laser operating at λ=633 nm. Thermal analysis was performed in air ona TG/DSC 1 Star System (Mettler-Toledo) coupled with MS-Thermostar GSD320 (Pfeiffer Vacuum) Mass Spectrometer). Fluorescence images of PNIPAM-CQDs@PEG were taken at ambient temperature on a Leica TCS SP5 Confocal (Leica). Samples were prepared by dropping a small amount of colloidal solution onto 1 x 1 cm^2 silicon wafers. We characterized the localized emission fluorescence between 550-650 nm, excited with a laser at 458 nm using 100 x objective. More details about the characterization methods are presented in Supplementary Information

Conclusions

In summary, we have synthetized by an easy procedure CQDs coated with PEG using a hydrothermal reaction. NMR, FTIR and XPS confirmed the grafting of CQDs nanoparticles with PEG. The intensity of the fluorescence emission of the CQDs@PEG nanoparticles was higher compared to that of unmodified CQDs in a range of excitation wavelength between 380-350 nm. Moreover, that maximum shifts from 455 to CQDs to 495 nm for CQDs@PEG particles. CQDs@PEG nanoparticles were treated with 3-BA, and they were incorporated within pNIPAM microgels (pNIPAM-CQDs@PEG**)** by free radical polymerization. The hybrid microgel showed photoluminescence and had a transition temperature similar to that for a system with an ionic component.

Acknowledgements

This work was supported by the projects P12-RNM-1565 (J. Andalucía (Spain) and CTQ2012-37925-C03-03 (MINECO, Spain). Authors thank the Ministry of Education, Science and Technology of the Republic of Serbia (Grant Nº 173017). BB Campos is gratefully to SFRH/BD/84318/2012fellowship (FCT, Portugal). RCC acknowledges the M. Curie COFUND programme "U-Mobility" co-financed by Univ. Malaga and the EU 7thFP Grant Agreement No 246550.We thank the financial support from ANPCYT (PICT 2012-0151), Univ. Buenos Aires (UBACyT 2013-2016/043BA) and CONICET (PIP 2014-2016/130).

Notes and references

1 H. Li, Z. Kang, Y. Liu, S. T. Lee. *J Mat Chem.,* 2012, **22,** 24230.
2 S. N. Baker, G. A. Baker, Angew. Chem. Int Ed., 2010, **49,** 6726.
3 Y. Wang, A. Hu, *J Mat. Chem. C*, 2014, **2,** 6921.
4 L. Cao, X. Wang, M. J. Meziani, F. Lu, H. Wang, P. G. Luo, Y. Li, B. A. Harruff, L. M. Veca, D. Murray, S. Y. Xie, Y. P. Sun, *J. Am. Chem. Soc.*, 2007, **129,** 11318.
5 M. Algarra, M. Pérez-Martín, M. Cifuentes-Rueda, J. Jiménez-Jiménez, J. C. G. Esteves da Silva, T. J. Bandosz, E. Rodríguez-Castellón, J. T. López-Navarrete, J. Casado, *Nanoscale,* 2014, **6,** 9071.
6 S. Chandra, S. Mitra, D. Laha, S. Bag, P. Das, A. Goswami, P. Pramanik, Chem. Commun., 2011;47:8587-8589.
7 S. T. Yang, L. Cao, P. G. Luo, F. Lu, F. Wang, H. Wang, M. J. Meziani, Y. Liu, Q. Qi, Y. P. Sun, *J. Am. Chem. Soc.,* **2009,** 31, 11308.
8 H. Li, X. He, Z. Kang, H. Huang, Y. Liu, J. Liu, S. Lian, C. H. Tsang, X. Yang, S. T. Lee, *Angew. Chem. Int. Ed.,* 2010, **49,** 4430.
9 M. Algarra, B. B. Campos, K. Radotić, D. Mutavdžić, T. J. Bandosz, J. Jiménez-Jiménez, E. Rodriguez-Castellón, J. C. G. Esteves da Silva, *J. Mat. Chem. A,* 2014, **2,** 8342.
10 C. López, M. Zougagh, M. Algarra, E. Rodríguez-Castellón, B. B. Campos, J. C. G. Esteves da Silva, J. J. Jiménez-Jiménez, A. Ríos, *Talanta,* 2015, **132,** 845.
11 Y. Dong, R. Wang, H. Li, J. Shao, Y. Chi, X. Lin, G. Chen, *Carbon,* 2012, 50, 2810.
12 K. A. S. Fernando, S. Sahu, Y. Liu, W. K. Lewis, E. A. Guliants, A. Jafariyan, P. Wang, C. E. Bunker , Y. P. Sun, *Appl. Mater. Interfaces,* 2015, **7,** 8363.
13 D. Mosconi, D. Mazzier, S. Silvestrini , A. Privitera, C. Marega, L. Franco, A. Moretto, *ACS Nano,* 2015, **9,** 4156.
14 S. Chandra, P. Patra, S. H. Pathan, S. Roy, S. Mitra, A. Lavek, R. Bhar, P. Pramanik, A. Goswani, *J Mater Chem B,* 2013, **1,** 2375.
15 O. Kozák, K. Kumara, R. Datta, M. Greplová, V. Ranc, J. Kašlík, R. Zbořil. *J. Phys. Chem. C,* 2013, **117,** 24991.
16 F. Wang, M. Kriter, B. He, S. Pang, C. V. Liu, *Chem. Commun.* 2010, **46,** 3309.
17 S. L. Hu, K. Y. Niu, J. Sun, J. Yang, N. Q. Zhao, X. W. Du, *J Mater Chem.*, 2009, **19,** 484.
18 X. Xu, R. Ray, Y. Gu, H. J. Ploehn, L. Gearheart, K. Raker, W. A. Scrivens, *J. Am. Chem. Soc.,* 2004, **126,** 12736.
19 L. Zheng, Y. Chi, Y. Dong, J. Lin, B. Wang, *J. Am. Chem. Soc.,* 2009, 131, 4564.
20 Q. L. Zhao, Z. L. Zhang, B. H. Huang, J. Peng, M. Zhang, D. W. Pang, *Chem. Commun., 2008*, 5116.
21 J. Lu, J. X. Yang, J. Wang, A. Lim, S. Wang, K. P. Loh, *ACS Nano,* 2009, **3,** 2367.
22 J. C. G. Esteves da Silva, H. M. R. Goncalves. *Anal. Chem.,* 2011, **30,** 1327.
23 Y. P. Sun, B. Zhou, Y. Lin, W. Wang, K. A. S. Fernando, P. Pathak, M. J. Meziani, B. A. Harruff, X. Wang, H. F. Wang, P. J. G. Luo, H. Yang, M. E. Kose, B. L. Chen, L. M. Veca, S. Y. Xie. *J. Am. Chem. Soc.,* 2006, **128,** 7756.
24 A. Sachdev, I. Matai, S. U. Kumar, B. Bhushan, P. Dubey, P. Gopinath. RSC Adv., 2013, 3, 16958.
25 Q. Li, T. Y. Ohulchanskyy, R. Liu, K. Koynov, D. Wu, A. Best, R. Kumar, A. Bonoiu, P. N. Prasad, *J Phys. Chem. C,* 2010, **114,** 12062.
26 C. Yu, X. Li, F. Zeng, F. Zheng, S. Wu, *Chem. Commun.,* 2013, **49,** 403.
27 H. Ding, L. W. Cheng, Y. Y. Ma, J. L. Kong, H. M. Xiong, *New. J. Chem.,* 2013, **37,** 2515.
28 Y. Q. Zhang, D. K. Ma, Y. Zhuang, X. Zhang, W. Chen, L. L. Hong, Q. X. Yan, K. Yu, S. M. Huang, *J. Mater. Chem.,* 2012, **22,** 16714.
29 C. Wang, N. T. Flynn. *Adv. Mater.,* 2004, **16,** 1074.
30 Y. Lu, Y. Mei, M. Drechsler, M. Ballauff, *Angew. Chem. Int. Ed.,* 2000, **45,** 813.
31 R. A. Álvarez-Puebla, R. Contreras-Cáceres, I. Pastoriza-Santos, J. Pérez-Juste, L. M. Liz-Marzan, *Angew. Chem. Int. Ed.,* 2009, **48,** 138.
32 M. Karg, I. Pastoriza-Santos, L. M. Liz-Marzán, T. Hellweg, *Chem. Phys. Chem.,* 2006, **7,** 2298.
33 N. Singh, L. A. Lyon, *Chem. Mater.,* 2007, **19,** 719.
34 M. Laurenti, P. Guardia, R. Contreras-Cáceres, J. Pérez-Juste, A. Fernández-Barbero, A. López-Cabarcos, J. Rubio-Retama, *Langmuir,* 2011, **27,** 10484.
35 Y. Q. Wang, Y. Y. Zhang, Z. Zhang, W. Y. Li, *J. Mater. Chem.,* 2011, **21,** 6556.
36 R. Contreras-Cáceres, S. Abalde-Cela, P. Guardia-Giros, A. Fernández-Barbero, J. Pérez-Juste, R. A. Álvarez-Puebla, L. M. Liz-Marzán. *Langmuir,* 2011, **27,** 4520.

View Article Online
DOI: 10.1039/C6NJ03893J

37 J.M. Lázaro-Martínez, E. Rodríguez-Castellón, D. Vega, G.A. Monti, A.K. Chattah. Macromolecules, 2015, **48**, 1115.
38 N. Baccile, G. Laurent, F. Babonneau, F. Fayon, M.M. Titirici, Antonietti. *J. Phys. Chem. C,* 2009, **113**, 9644.
39 B. De and N. Karak. *RSC Adv.* 2013, **3**, 8286.
40 F.S. Asghari, H. Yoshida H. *Ind. Eng. Chem. Res.* 2005, **45**, 2163.
41 J.M. Lázaro-Martínez, P.N. Romasanta, A.K. Chattah, G.Y. Buldain. *J. Org. Chem*. 2010, **75**, 3208.
42 Y.G. Linck, A.K. Chattah, R. Graf, C.B. Romañuk, M.E. Olivera, R.H. Manzo, G.A. Monti, H.W. Spiess. *Phys. Chem. Chem. Phys.*, 2011, **13**, 6590.
43 D. Mutavdžić, J. Xu, G. Thakur, G. Triuli, S. Kasas, S. Jeremić, R. Leblanc, K. Radotić. Analyst, 2011, **136**, 2397.
44 H. Zhu, H. Wang, Y. Li , Z. Wang, F. Yang, X. Yang, *Chem. Commun.,* 2009, 5118.
45 S. Hirotsu, *Phase Trans,* 1994, **47,** 183.
46 R. Contreras-Cáceres, J. Pacifico, I. Pastoriza-Santos, J. Pérez-Juste, A. Fernández-Barbero, L. M. Liz-Marzan. *Adv. Funct. Mater.,* 2009, **19,** 3070.
47 G. Weber, F.W.J. Teale. *Trans. Faraday Soc.* 1957, **53**, 646
48 A.M. Brouwer. *Pure Appl. Chem.* 2011, **83**, 2228.